"Manufacturing and characterization of hybrid composites with basalt and flax fabrics and a partially bio-based epoxy resin"

D. Lascano[1], R. Balart[2], D. Garcia-Sanoguera[2], A. Agüero[2], T. Boronat[2], N. Montanes[2]

[1] Escuela Politécnica Nacional, 17-01-2759, Quito, Ecuador; dielas@epsa.upv.es (D.L.).

[2] Technological Institute of Materials (ITM), Universitat Politècnica de València (UPV), Plaza Ferrándiz y Carbonell 1, 03801 Alcoy, Spain; dagarsa@dimm.upv.es (D.G-S); rbalart@mcm.upv.es (R.B.); anagrod@epsa.upv.es (A.A.); nesmonmu@upvnet.upv.es (N.M.); tboronat@dimm.upv.es (T.B.).

* Correspondence: dielas@epsa.upv.es; Tel.: +34-966-528-433.

Running title

Manufacturing of bio-based hybrid composite laminates by VARIM

Abstract

This research is focused on manufacturing and characterization of hybrid composite laminates obtained different stacking sequences of basalt and flax fabrics with silane treatments embedded in a partially bio-sourced epoxy resin as matrix. They were manufactured by the vacuum-assisted resin infusion molding and mechanical properties were tested in tensile, flexural and impact conditions. The effect of the coupling agent on the fiber/matrix interface was studied by FESEM. The effect of temperature on mechanical properties was evaluated by DMTA and TMA. FESEM images revealed improved fiber/matrix interactions with silane treatment, having a more satisfactory effect on basalt fibers than on flax fibers because of its silica-based structure, leading to improved mechanical properties. It is worthy to note that the hybrid stacking sequence has no remarkable influence on the elongation at break. On the contrary, the hybrid stacking sequence offered a great influence on both the elastic modulus and the tensile strength.

Keywords: bio-based epoxy resin; hybrid composites laminates, VARIM.

1. Introduction.

Composite materials are one of the most promising areas of thermosetting polymers. Conventional fibers such as carbon, aramids, and glass, offer superior mechanical properties to most materials and this has led composite materials into advanced materials sectors and high-performance applications. Some of their outstanding properties are lightness, high Young's modulus, high tensile strength and good thermal stability, among others [1-3]. When these fibers are used as reinforcements embedded into a polymeric matrix (usually a thermosetting polymer), the obtained composite materials offer a synergistic improvement in both manufacturing and final properties. These composites are lightweight technical materials with growing uses in advanced industrial sectors such as aerospace, aeronautics, automotive, medical devices and equipment, or construction sector [4-6]. The excellent performance of these materials allows them to substitute other conventional materials such as steel in civil applications [7]. Despite these notorious qualities, the overall cost of these fibers, mainly carbon and aramids is still high due to complex manufacturing processes [8]. To overcome the cost-related problem, some efforts have been done to totally or partially replace the content of these fibers in composite materials or laminates, aiming a good balance between performance and cost. In the last decade, most research works have focused on the potential of hybrid composite materials laminates with different fibers/fabrics in a particular stacking sequence. Artemenko *et al*. [9], reported a hybrid composite with carbon and glass fibers, with the subsequent cost reduction. Nevertheless, the decrease in mechanical properties was noticeable. In particular, these hybrid carbon/glass composites showed a flexural strength 40% lower than carbon fiber composites. Marom *et al*. [10], manufactured hybrid composite laminates with aramid (Kevlar®) and carbon fiber, achieving hybrid materials with good impact absorption properties when Kevlar plies were located in the outer layers of the composite material.

In addition to the cost reduction, in the last decade the increasing concern about environment is leading the change to the use of environmentally friendly materials and processes. In accordance to this tendency, the use of natural fibers has emerged as an interesting alternative to give high environmental efficiency materials. Natural fibers are obtained from renewable resources which represents a notorious advantage from a production standpoint [11], and a positive effect on reducing greenhouse gases emissions. The most used fibers in the manufacture of composite materials are jute, hemp, cotton and flax, among others [12, 13]. One of the most interesting fibers for the composite's industry is flax. Due to its composition, which is mostly made up of helical structures (microfibrils) of cellulose, flax fibers can provide high tensile strength and modulus. The microfibril orientation in flax fibers is 10º, and the cellulose content is around 71%, which can lead to values of the tensile strength of up to 1129 MPa [14]. Several authors have devoted themselves to the study of hybrid structures between synthetic fibers and natural fibers. Zhang *et al*. [15], reported interesting properties on hybrid composite materials with flax and glass fibers. The showed good interaction between the fibers since fracture toughness and interlaminar shear strength turned out to be higher compared with composite laminates with glass fibers. Morye *et al.* [16], reported an increase in the flexural an impact strength properties on hybrid composites of flax and glass fibers. Ramesh *et al*. [17] studied the hybrid effect of synthetic fibers such as carbon and natural fibers such as hemp. Natural fibers were pre-treated with alkaline solutions, which determined that the pre-treatment increased the mechanical properties compared to untreated fibers, and also caused water absorption to decrease. Bajpai *et al.* [18] developed safety helmets based on hybrid fiberglass and jute fiber materials embedded in an epoxy resin matrix. It was determined that the flexural properties were superior when the fiberglass content was lower, allowing these materials with a high percentage of natural fibers to replace conventional materials such as ABS. Palanikumar *et al.* [19] developed hybrid compounds based on sisal and glass fibers, where the incorporation of 20% sisal fibers worked better and the hybrid effect was greater, resulting in increased mechanical properties in tensile and bending. Making them an option for composites made entirely of glass fibers.

As an alternative to glass fibers, it is possible to find some different siliceous fibers with interesting properties from a technical point of view. These fibers are obtained from mineral products such as rocks, therefore, these fibers are known commercially as rock wool, depending on the type of rock [20]. Among the rocks used for this purpose, basalt is the most promising. This rock is the result of the cooling of magma on the earth's surface [21]. Due to its particular structure, processing of basalt rocks is much simpler, cheaper and with less environmental impact than production of glass fibers, which generates too much waste [22]. Properties such as low or no chemical reactivity, good thermal behavior, good mechanical properties, high modulus, are some of the features of basalt fibers [23, 24]. Dehkordi *et al*. [25] reported improved buckling strength when subjected to high impact energies on hybrid composites of basalt-nylon intraply fabrics. Matykiewicz *et al*. [26] reported the thermomechanical properties of hybrid composites of basalt fibers and basalt powder. The hybrid composition achieved a synergistic effect by improving the thermal resistance and the stiffness of the composite. Several authors have studied the hybrid effect with natural fibers, Matykiexicz and Barczewski [27] prepared a hybrid composite with basalt and flax fibers pre-treated with silanes embedded in an epoxy resin and basalt powder matrix. They determined that the mechanical properties of the composites were not affected by the incorporation of the flax fibers and that the silane-based treatment worked well, resulting in a better fiber-matrix interface and increased composite stiffness. Sergi *et al*.

[28] investigated the effect of water aging and UV radiation on hybrid compounds based on basalt and hemp fibers in a thermoplastic matrix of high-density polyethylene modified with maleic anhydride. Where the hybrid effect worked well since after accelerated aging the mechanical properties improved, also causing water absorption to decrease. Despite the good properties of these fibers, the interaction between them and the surrounding thermosetting matrix is usually deficient, resulting in a marked decrease in mechanical properties, since the loads are not transmitted correctly to the fibers [29, 30]. To improve this interaction, different types of treatments are usually performed to selectively modify the fiber surface. Different physical and chemical processes have been proposed to overcome this drawback. Among all these treatments, silanization seems to be the most effective from both technical and economic considerations [31]. The dual functionality of silanes allows formation of bridges between the fiber surface and the thermosetting polymer matrix [32].

Typical thermosetting resins for composites include unsaturated polyesters (UP), epoxies (EP), phenolics (PF), vinyl ester (VE), among others. Epoxies are widely used in engineering due to excellent properties they can provide [33, 34]. conventional epoxies for composites are based on diglycidyl ether of bisphenol A, DGEBA [35, 36]. DGEBPA epoxies are petroleum-based materials and substantially contribute to increase the carbon footprint. With the aim of reducing this, different bio-based materials have been proposed [37, 38], mainly derived from non-edible vegetable oils (VO) [39]. The particular structure of vegetable oils, based on a triglyceride with three different fatty acids allows some chemical modifications, especially on unsaturated fatty acids such as oleic, linoleic and linolenic acids [40].

The purpose of this research is assess the potential of hybrid composite laminates of flax and basalt fibers embedded into a partially bio-based epoxy resin, obtained by vacuum assisted resin infusion molding (VARIM). This work also covers the study of the interaction between basalt and flax fibers subjected to a silanization process. In addition, the stacking sequence of flax and basalt fabrics on composite laminates is evaluated in terms of mechanical performance.

2. Experimental

2.1. Materials.

The matrix was a partially bio-based epoxy resin, commercial grade Resoltech® 1070 ECO and an amine-based hardener type Resoltech® 1074 ECO, both of them supplied by Castro Composites (Pontevedra, Spain). The epoxy resin is based on diglycidyl ether of bisphenol A (DGEBA) with 31% of plant-based reactive diluent. It provides good UV stability and high mechanical properties. The ratio between the epoxy resin and the hardener was 100:35 respectively (parts by weight), as recommend the manufacturer. Two types of fabrics were used to manufacture hybrid composite laminates. Basalt fabric BAS 940.1270.T supplied by Basaltex (Wevelgem, Belgium) with a specific surface weight of 940 g cm^{-2} and Biotex Flax fibers supplied by Composites evolution (Chesterfield, United Kingdom) with a specific surface weight of 400 g cm^{-2}. Some properties of flax fiber and basalt fiber fabrics are summarized in **Table 1**, all fabrics present a compensated setup on weft and warp directions. The glycidyl-functional silane (3-glycidyloxypropyl) trimethoxysilane was used as a coupling agent and was obtained from Sigma-Aldrich (Madrid, Spain).

Table 1

2.2. Pre-treatment of fibers.

In order to remove any external agents (sizings), which can interfere with the manufacturing process of basalt/flax composite laminates, basalt fabrics were initially washed in a distilled water bath and then subjected to a thermal program at 300 ºC for 3 h to remove any organic sizing.

In order to improve the surface interaction between the reinforcing fibers and the thermosetting matrix, both basalt and flax fabrics were subjected to a silanization treatment. The aqueous solution for this treatment contained 1 wt% silane. Then the solution was magnetically stirred for 2 hours at room temperature until homogenization. Then, the corresponding fabrics were immersed in this solution for 2 hours at room temperature. After this stage, the fabrics were removed from the bath and were dried at 80 °C for 12 hours.

2.3. Manufacturing of hybrid basalt/flax composite laminates.

Manufacturing process of basalt/flax/epoxy composites was carried out by the VARIM process (Vacuum Assisted Resin Infusion Molding). This method consists on a conventional infusion process assisted by vacuum. VARIM process follows different stages. First, basalt and flax fabrics with different stacking sequences as summarized in **Table 2**, were placed on a board coated with a thin layer of a release agent (polyvinyl alcohol) as it is shown in **Scheme 1a,** all layers are biaxial fabrics $[0/90]_{2S}$. Then, a peel-ply sheet was placed above the stacked fabrics followed by the bleeding fabric, to ensure good resin flow and spreading (**Scheme 1b**). Then, the system was sealed with a plastic bag with double-side sealing tape. Finally, the resin inlet and the vacuum outlet were placed appropriately (**Scheme 1c**). Then the vacuum was tested to ensure no leaking. Once this stage was checked and it was confirmed there was no leaking, the resin was infused thus embedding all fabrics (**Scheme 1d**). After the infusion, the hybrid composites were subjected to a curing cycle of 1 h at 80 ºC and a subsequent post curing cycle at 125 ºC for 30 min.

Table 2

Scheme 1

2.4. Mechanical properties of laminate composites.

Mechanical properties of hybrid basalt/flax epoxy composite laminates with bio-based epoxy resin were evaluated in flexural and impact conditions. The flexural test was performed following the guidelines of ISO 178 standard; the crosshead rate was set at 5 mm min^{-1}. Flexural test was performed on an electromechanical universal testing machine ELIB 50 from S. A. E. Iberest (Madrid, Spain), with a 50 kN load cell. Impact strength was evaluated by the Charpy test, following the guidelines of ISO 179 standard in a Charpy pendulum from Metrotec (San Sebastián, Spain), using a 6 J pendulum on notched samples (“U” type, 2 mm depth and a radio of 0.5 mm) as it is shown in **Figure 1**. All tests were conducted at room temperature with at least five samples of each laminate. The average values of the corresponding parameters of each test were calculated.

Figure 1

In order to have a better understanding of the effect of the hybrid structure of composite laminates on toughness, a conventional tensile test with the same notched samples (**figure 1**) used for impact tests was carried out. This tensile test was carried out in a ELIB 50 from S. A. E. Iberest (Madrid, Spain), with a 50 kN load cell and the crosshead rate was set to 3 mm min^{-1}. This test allows calculating the area below its characteristic tensile diagram, which is directly related to overall toughness. The main parameters obtained from this test were the maximum tensile strength and the area below the tensile curve. Five different samples were tested, and the corresponding values were averaged, in addition, longitudinal and cross-sectional data have been considered.

2.5. Thermomechanical characterization

Thermomechanical properties of hybrid basalt/flax composite laminates with bio-based epoxy resin were evaluated by dynamic mechanical thermal analysis (DMTA).

An oscillatory rheometer AR-G2 from TA Instruments (New Castle, USA) equipped with a clamp system for solid samples working in torsion-shear conditions was used. The samples had a rectangular shape size of 40 x 10 x 4 mm^3. The heating program was a temperature sweep from 30 ºC up to 200 ºC at a constant heating rate of 2 ºC min^{-1}. The maximum shear/torsion deformation (γ) was defined as a percentage of 0.1% and the selected frequency for the oscillations was 1 Hz.

Additionally, to the dynamic characterization of basalt/flax hybrid composites by DMTA, their dimensional stability was analyzed by obtaining the coefficient of linear thermal expansion (CLTE) in a thermomechanical analyzer (TMA) Q400 from TA Instruments, using square samples (10x10 mm^2) with a variable thickness from 7 to 11 mm, with parallel faces. The dynamic heating program was scheduled from 30 ºC up to 170 ºC to cover the range in which the T_g of the epoxy is expected. A constant heating rate of 2 ºC min^{-1} was used with a constant load of 20 mN.

2.6. Fiber/matrix interaction and morphology analysis.

The interaction between basalt fibers and flax fibers with the epoxy resin matrix in hybrid basalt/flax composite laminates was analyzed by field emission scanning electron microscopy (FESEM), in a ZEISS ULTRA 55 FESEM microscope from Oxford Instruments (Abingdon, United Kingdom) working at an acceleration voltage of 2 kV. Prior to observation by FESEM, all samples were coated with an ultrathin gold-palladium layer in a high vacuum sputter coater EM MED20 from Leica Microsystem (Milton Keynes, United Kingdom), to provide electrical-conducting properties to samples. In addition, the morphology of the fractured surfaces from fractured specimens from impact test was observed using a stereomicroscope system SZX7 model from Olympus (Tokyo, Japan). It was equipped with a KL 1500-LCD light source.

2.7. Statistical Analysis.

The data obtained when analyzing the different properties of epoxy basalt/flax composite laminates were evaluated with a $p<0.05$ (95%) confidence interval using an analysis of variance (ANOVA). The OriginPro8 software (OriginLab Corporation, Northampton, MA, USA) was used to perform the Tukey multiple comparison tests.

3. Results and discussion.

3.1. Morphology of untreated and silanized basalt and flax fibers.

Mechanical properties of composites are directly related to fiber/matrix interactions. Strong fiber/matrix interactions allow load transfer from the matrix to the reinforcing fiber and this has a positive effect on overall mechanical performance. On the contrary, poor fiber/matrix interactions are responsible for poor mechanical properties due to poor material's cohesion. The surfaces of the reinforcing fibers after the silane treatment were analyzed by field emission scanning electron microscopy (FESEM); these images are displayed in **Figure 2.** Both **Figure 2(a)** and **Figure 2(b)**, show basalt fiber surface as-received, without any treatment. It can be noticed that the surface has some impurities, which appear in the form of roughness on these surfaces. This roughness is no more than the protective sizing of basalt fibers. This sizing is usually added to facilitate their handling during manufacturing due to its brittleness. Flax fibers, unlike basalt fibers, do not have a uniform surface, they have a fluted structure, generally having between 5 and 7 lateral sides as indicated in **Figure 2(c)** and F**igure 7(d)**, which is quite typical of natural fibers, as this particular shape allows packing fibers [16]. **Figure 2(e)** and **Figure 2(f)** show the surfaces of basalt fibers subjected to cleaning and subsequent heat treatment at 300 ºC to remove organic sizings. The results obtained after this process is notorious as the initial roughness of untreated basalt fibers has almost disappeared, resulting in completely smooth surfaces, meaning that the initial sizing of the basalt fibers has been removed. This is necessary due to the presence of undesired elements such as binders, sizings dirt, and others, which are usually present in the surface of basalt fibers. Some of these chemicals are needed to appropriately manufacture the highly brittle basalt fibers. If these chemicals and/or dirt are not removed, the silanization process lose its effectiveness because these elements prevent anchoring between the hydroxyl groups of the fibers on their surface and the hydrolyzed silanol groups contained in the glycidyl-functional silane (3-glycidyloxypropyl), as observed in previous studies [41], so that it does not cause subsequent failures while manufacturing composite laminates and, moreover, allows good anchorage of silane after silanization. The effect of silanization on both fibers can be seen in **Figure 2(g)** and **Figure 2(h)** for basalt and in **Figure 2(i)** and **Figure 2(j)** for flax fibers. As it can be seen for both fibers, the surface roughness has increased which is due to formation of a thin layer of silane that has been strongly adhered to the fibers in a similar way as reported by Park *et al.* [42] and Samper *et al.* [29].

Figure 2

3.2. Mechanical properties and morphology of basalt/flax hybrid composite laminates.

The mechanical behaviour of basalt/flax hybrid laminates was studied through flexural and Charpy tests (as an estimation of the toughness). The values obtained by the different mechanical tests are summarize in **Table 3**. It is noteworthy that the high values obtained for flexural strength and impact strength are mainly due to the effect provided by the coupling agent as observed in other similar composite laminates [43-45]. It can be seen that the flexural strength (σ_f) and flexural modulus (E_f) for B8F0 laminate are 467.9 MPa and 14.7 GPa respectively, which are relatively high due to the stiff properties of basalt fiber which are comparable to those of glass fibers and slate fibers as reported by Samper *et al.* [46]. In addition, this is due to the great affinity that these types of fibers have with a polymeric matrix after silanization process, in this case, with a glycidyl silane which can readily react with the epoxy resin. On the contrary, as flax fiber is characterized by remarkably lower mechanical properties, the B0F8 composite laminate offers a flexural strength of 51.5 MPa and a flexural modulus of 2.2 GPa which are close to some engineering plastics. It is evident that this composite laminate with all-basalt fabrics (B8F0) is the one with the highest flexural strength and modulus but it is possible to substitute some basalt fabrics with flax fabrics, which leads to increased environmental efficiency and balanced mechanical properties. For example, the B6F2 composite laminate, with two flax plies offers high flexural properties of 307.7 MPa (flexural strength) and 12.2 GPa (flexural modulus) which can compete with some conventional glass fiber composites. Even the composite with 4 flax plies and 4 basalt plies (B4F4) shows interesting mechanical performance, with a flexural strength of 241.9 MPa and a flexural modulus close to 10 GPa (9.5 GPa). This increase in flexural properties can be attributed to the good synergy that the reinforcement fibers have with the matrix because of the treatment with coupling agents carried out before their manufacture, as above-mentioned. Usually, polymer-matrix interactions are not good enough to guaranty load transfer, and this results in poor or decreased mechanical properties. Nevertheless, coupling agents such as silanes, as they possess dual functionality, they can react/interact with both the thermosetting matrix and the reinforcing fiber and, positively contribute to load transfer, with a subsequent positive effect on mechanical properties. The literature presents hybrid materials in which the incorporation of glass fiber resulted in flexural properties similar to those obtained in this work [47, 48], making this a potential environmentally friendly alternative for some glass-fiber composites in many applications. It is important to remark that even with the same number of flax and basalt pies, B4F4 and B4F4alt composite laminates offer remarkably different flexural properties. In B4F4 composites, basalt fabrics are located in the external plies of the symmetric laminates (see **Table 2.**) This stacking sequence provides increased stiffness and strength. On the contrary, the B4F4alt composite laminate, contains one external basalt ply and two internal (in the middle) basalt plies; so that, flax fiber acts as the principal reinforcement material thus leading to decreased mechanical properties. In particular, the flexural strength and modulus for the B4F4alt laminate are 156.5 MPa and 4.0 GPa which are almost half the values of the B4F4 stacking sequence. As reported by Park and Jang [49], in hybrid carbon/polyethylene composites, the stacking sequence and the relative position of the carbon plies play a key role on final performance. As the flax ply number increases, it is detectable a decrease in flexural performance but even for the B2F6 composite laminate, the flexural strength is interesting (129.7 MPa) with a flexural modulus of 6.4 GPa. These properties are typical of engineering plastics reinforced with short glass and/or carbon fibers [50, 51], thus giving an alternative to the high cost of these engineering plastics and, what is more interesting, providing increased environmental efficiency.

With respect to the impact strength obtained by the Charpy test, **Table 3** shows the effect of hybridization on toughness, measured as the impact strength. In a similar way to flexural properties, the highest impact strength is obtained for the all-basalt composite (B8F0) with and absorbed energy of 116.9 kJ m^{-2}. This impact energy is relatively high compared to other composite laminates. For example, Samper *et al.* [46] reported an impact strength of almost 80 kJ m^{-2} in composites with slate 4 plies embedded into an epoxy resin, using a glycidyl silane as coupling agent. Basalt laminates offer superior impact strength properties. As some basalt plies are exchanged by flax plies, the impact strength decreases down to values of 9.0 kJ m^{-2} for the all-flax composite laminate (B0F8) which indicates very low energy absorption, even lower than some engineering plastics, such as PBSA injected samples (26 kJ m^{-2}), PCL/PHB binary blends with 75% of PCL and 25% of PHB (11 kJ m^{-2}), and LDPE injected specimens (53 kJ m^{-2}) [52-54]. It should be noted that composite laminates made by four basalt plies and four flax plies show relatively high values for the impact strength (B4F4alt), of 77.8 kJ m^{-2}. Once again, composite laminates with the same number of basalt and flax plies but with different stacking sequences show different behaviour. As indicated previously, flax plies are not good energy absorbers; for this reason, the B4F4 shows slightly lower energy absorption than the B4F4alt, with values of 64.0 kJ m^{-2} and 77.8 kJ m^{-2} respectively. In B4F4 composite, the outer plies are basalt fabrics and they can absorb some energy in the initial stages of the impact process. Once the basalt fabrics are broken, flax plies do not offer high resistance to deformation thus leading to slightly reduced impact strength values compared to B4F4alt. In this last case, an outer basalt ply receives the impact and breaks and then, immediately, flax fibers are exposed to impact with very low energy absorption but this stacking sequence contains two basalt plies in the middle which are able to absorb energy once the pendulum has lost some of its initial impact energy and this gives slightly higher impact strength. In addition, when the strongest fibers are located at the skin region (outer plies), they can withstand high tensile and compression stresses during the impact and this positively contributes improved toughness as reported by Ary Subagia *et al*. [55]. It is possible to observe similar results in different hybrid composite structures in which, the stacking sequence is a key parameter on final performance of composite plates; in general when the stiffer and strongest plies are located in the skins (outer plies), flexural and impact properties are remarkably improved [56].

Table 3

Energy absorption and subsequently, toughness, is key parameter on selecting materials for engineering applications. For this reason, an additional estimation of the toughness has been carried out by tensile tests with the same samples used for impact tests. **Figure 3** gathers a comparative plot of the stress-strain diagrams obtained for basalt/flax hybrid composite plates. The area below the characteristic stress-strain curve is representative for the overall toughness or the absorbed energy during the deformation and fracture of composite plates. All composites show a linear behaviour until fracture occurs. The most relevant information obtained from this test is summarized in **Table 4**. As one can see, a simple observation of **Figure 3** indicates that the all-basalt composite plate is, with difference, the one with the highest toughness, measured as the area below the stress-strain curve. In particular, this area is 25.06 MN m m^{-3} which is remarkably higher than the area below the stress-strain curve for all-flax composite plate (B0F8), which is 1.77 MN m m^{-3}. These units, *i.e.* MN m m^{-3}, suggest energy or work (MN m) units per volume fraction (m^{-3}), so that, it is possible to use this value as an estimation of the energy absorbed until failure. As expected, when some basalt plies are exchanged by flax plies, the area below the σ–ε diagram decreases as basalt is much tougher than flax. These results are in total agreement with those obtained by the conventional Charpy test. Nevertheless, with regard to composites with the same number of basalt and flax plies with different stacking sequences (B4F4 and B4F4 alt), it is possible to observe some differences with the results obtained by the Charpy test. Although there is a correlation between these two tests, the conditions are, obviously, different since the Charpy considers energy absorption in a very short period of time (impact) while the tensile test offers the energy absorption in a larger period of time. Therefore, it is possible to conclude that the way the load is applied can influence the final energy absorption as in this case. With regard to the maximum stress before failure occurs, **Table 4** shows the same tendency observed by flexural tests. The maximum stress value for the notched sample in this tensile test corresponds to the B8F0 laminate with a value of 211.9 MPa. On the contrary, the lowest value can be detected for the all-flax composite (B0F8) with a maximum tensile stress of 21.7 MPa. As the basalt plies are exchanged by flax plies, the maximum tensile stress decreases.

Figure 3

Table 4

The fractured surfaces of the hybrid composite plates from impact tests were observed by FESEM in order to assess the effectiveness of the coupling agent in terms of the interface phenomena of the reinforcing fibers and the polymer matrix. The polymer-fiber interface gives an idea of the effect of the coupling agent treatment on mechanical properties. **Figure 4a** and **4b** correspond to the fracture of the all basalt (B8F0) composite laminate. It can be observed that there are no discontinuities between the matrix and the surrounding fibers, that is, which indicates good wettability of the fiber resin with the resin. This is because the coupling agent (glycidyl silane) has an epoxy functionality that can react with both basalt fiber and epoxy matrix. The coupling between the glycidyl silane and the basalt fiber takes place by the condensation reaction of the hydrolyzed silane and the hydroxyl groups in the outmost layers of basalt fiber. This chemical anchorage of the silane onto the basalt fiber is achieved during the pre-treatment stage, and there is still a glycidyl group which can be able to react with the epoxy resin during the crosslinking. For this reasons, coupling agents act as a physical bridges between the fibers and the matrix and this allows good material's cohesion and continuity which has a positive effect on mechanical performance as described by España *et al*. [57]. As one can see, the individual fibers show a very rough surface which corresponds to the failure of the epoxy matrix instead of fiber debonding or pull-out, which is indicating good interface interactions as reported by Samper *et al.* [46]. The fracture surface corresponding to all-flax composite plate (B0F8) is shown in **Figure 4c** and **4d**. As it can be seen, there are some small gaps around the flax fibers, which leads to poor interaction between the fiber and the epoxy resin. This is indicating that the fiber is not well embedded into the epoxy resin, even with the previous silanization process. As reported by Bertomeu *et al.* [58], in flax/epoxy composites, the gap around the fiber and the surrounding matrix can be reduced by using conventional silanization treatment on flax fabrics; nevertheless, this gap does not disappear. The presence of these gaps does not allow right load transfer from the epoxy matrix to the flax fiber, and this has a negative effect on final properties. In addition, it is important to bear in mind that the mechanical properties of flax fibers are remarkably lower than those of basalt fibers, and all this has an effect on final performance of all-flax composites [59, 60].

Figure 4

In order to better ascertain the characteristics of the fractured surfaces of the hybrid composite laminates from impact test, fractured surfaces were also observed by optical stereomicroscopy with different ocular magnifying glasses. **Figure 5** gathers the cross-section and the fracture surfaces from impact tests corresponding to the different hybrid composite laminates. The fractured surface of the all-basalt B8F0 composite plate is displayed in **Figures 5b** and **5c** which shows the fracture surface is the result of a low matrix resistance (rigid epoxy matrix) compared to the strong basalt fiber. It is possible to see that the fibers exhibit small tearing areas at their fracture points, which is representative for a brittle behaviour of basalt fibers [42]. This is an indication of the strength these fibers provide to composites and this agrees with the above-mentioned impact-absorbed energy values which were the highest for B8F0 composite plate, due mostly to the excellent mechanical properties of the basalt fiber and the good fiber/matrix interface achieved after the silanization, as observed in the FESEM analysis. For hybrid composites, the fractured surface always shows the same morphology. As it can be seen in **Figures 5e** and **5f**, corresponding to the hybrid B6F2 composite plate, the fracture is caused by the premature failure of the flax fibers, since these present a lower pull-out length compared to the basalt fibers. This is due to their lower strength compared to basalt fiber as reported in literature [61, 62]. Although the interface between the flax fiber and the epoxy matrix is good enough, there is poor interaction with basalt plies and, therefore, these laminates show small gaps between the flax and basalt plies, causing delamination failure at the interface. On one hand, this poor interlaminar interaction can be caused by the manufacturing process since, the behaviour of both fibers with the epoxy resin is completely different. On the other hand, the silanized basalt fibers stablish strong interactions with the epoxy resin while the highly porous flax fiber absorbs more epoxy resin and this leads to a heterogeneous epoxy distribution in the plies. The same comments can be done for hybrid composite plates with different stacking sequences as shown in **Figure 5** with increasing the number of flax plies: **Figures 5h** and **5i** (B4F4), **Figures 5k** and **5l** (B2F6). In all these composites, flax fabrics fails before basalt fabrics. **Figures 5q** and **5r** show the fractured surface all-flax B0F8 composite laminate. Despite the fiber/matrix interface interaction was relatively good, the presence of interlaminar gaps was greater, which resulted in a decrease in its mechanical properties as described previously. Jusoh *et al.* [63] suggested that the different nature of natural and basalt fibers resulted in poor interfacial bonding. Possible premature delamination of the layers may be caused by an internal failure of the interlayer as occurred in laminates made with glass and flax fibers, and with glass and jute laminates, that presented a high degree of stretching causing the fibers to pull out during fracture.

Figure 5

3.2. Thermal and thermomechanical properties of basalt/flax hybrid composite laminates.

Regarding to the dynamic mechanical thermal behaviour (DMTA) of hybrid basalt/flax composite laminates, **Figure 6** gathers the comparative plots of the storage modulus (G′) and the dynamic damping factor (tan δ) with respect to temperature. **Table 5** includes some characteristic values of G′ at 60 ºC and 125 ºC as to compare the dynamic performance of the hybrid composites. **Figure 6a** shows the evolution of the storage modulus (G′) as a function of the increasing temperature. It is important to bear in mind that the storage modulus is directly related to the stiffness of the material and its elastic behaviour (ability to storage energy when dynamically loaded). It can be seen that all-basalt B8F0 composite plate has a G′ value of 1.78 GPa at a temperature of 60 ºC. Above this temperature, between 70 ºC and 110 ºC a remarkable decrease in G′ (about two-fold decrease) can be observed, which is attributable to the α-relaxation of the epoxy resin or its glass transition temperature (T_g). The α-relaxation in crosslinked thermosetting resins is directly related chain mobility. Below the α-relaxation, the chain mobility into the 3D crosslinked epoxy resin is highly restricted. Nevertheless, above the α-relaxation, the material behaves as a rubber like material and this is a clear evidence of the structure relaxation. Although the crosslinked structure is not lost, some segments can move, vibrate, and so on, leading to this rubbery behaviour. The internal structural stresses due to the fully crosslinked epoxy resin, is relaxed at moderate-to-high temperatures, thus indicating a transition from a rigid state to a rubbery state, which is representative for the glass transition temperature (T_g) this movement is made between the crosslinking points in the glass-to-rubber transition, and this is related to the *tan δ* peak [64]. As one can see, a clear decrease in G′ takes place during the α-relaxation or T_g. For example, for the B8F0 composite plate, the G′ value below T_g (at 60 ºC) is 1.78 GPa and this is reduced down to values of 98.4 MPa above the T_g (at 125 ºC). This indicates that below T_g the material behaves as a stiff and rigid material while above the T_g, the material has become soft. The hybrid stacking sequence has a clear effect on G′. The G′ curve for the all-basalt B8F0 composite laminate corresponds to the highest values of the developed materials. As the flax content increases in hybrid basalt/flax composites, these plates become less stiff and, subsequently, the G′ characteristic curves are shifted to lower values. The shape of the curve is the same but all the curves are moved down which indicate softer composites [16]. This corroborates the data obtained by flexural tests; by increasing the number of flax fibers layers the material's stiffness decreases. The lowest storage modulus corresponds, as expected, to the all-flax B0F8 composite plate with a value of G′ of 0.57 GPa at 60 ºC. **Figure 6b** shows the evolution of the dynamic damping factor which is a measure of the lost energy to the stored energy ratio, tan (δ) with increasing temperature. The glass transition temperature (T_g) is gathered in **Table 5.** Despite there are several criteria to obtain the T_g, one of the most recognized methods is that based on the peak maximum for the dynamic damping factor. The glass transition temperature corresponds to the matrix (epoxy resin), and, as it can be observed, there is not a remarkable change for all hybrid basalt/flax composites ($p<0.05$). The T_g is highly dependent on several factors such as the type of epoxy resin, the functionality, the hardener, the curing cycle, the use of a post-curing cycle, the use of accelerators, among others [65-67]. Varley *et al.* [68] have reported a T_g value of a partially bio-based epoxy resin of about 90 ºC after a curing and a post-curing cycle. They reported that reinforcing fibers (with or without a previous surface treatment) do not affect in a remarkable way the T_g.

Figure 6

The dimensional stability has been determined through the estimation of the coefficient of linear thermal expansion (CLTE) below and above T_g of all composite laminates in this study. As it can be seen in **Table 5**, the CLTE of all laminates below T_g is comprised between 250 μm m^{-1} K^{-1} and 260 μm m^{-1} K^{-1}, and although small changes can be observed, they are comprised within the standard deviation (lower than 10%). These values are typical of a glassy state as the CLTE is directly related to the deformation ability [58]. Above the T_g it is possible to see some differences; both all-basalt and all-flax composite laminates show a CLTE of 296.0 μm m^{-1} K^{-1} and 273.2 μm m^{-1} K^{-1}, respectively, while all hybrid composites show slightly higher CLTE comprised between 320 – 370 μm m^{-1} K^{-1}. This phenomenon above T_g has been observed by Gupta *et al*. [69] that suggested an additional expansion of the rubber state compared to the glassy state.

Table 5

4. Conclusions.

This work has assessed the potential of hybrid basalt/flax composite laminates with a partially bio-based epoxy resin for applications in engineering. These composite laminates can be manufactured by the vacuum assisted resin infusion moulding (VARIM) with excellent reproducibility. A previous treatment of both basalt and flax fabrics gives enhanced mechanical properties on composites. Obviously, the all-basalt composite laminate (8 basalt plies) shows the maximum flexural strength and modulus of 467.9 MPa and 14.7 GPa respectively. But the most important findings of this work is that hybrid composite laminates containing different flax plies can give interesting properties from a technical point of view. It is worthy to remark the high flexural strength and modulus of hybrid composites containing 2 flax plies and 6 basalt plies (307.7 MPa and 12.2 GPa respectively) and the composite with 4 flax plies and 4 basalt plies with a flexural strength of 241.9 MPa and a flexural modulus of almost 10 GPA. These properties allow the use of these composites as potential substitutes of glass and basalt composites in technical applications. In addition, hybrid basalt/flax composites give improved environmental efficiency that can positively contribute to a sustainable development in the field of composite materials. It is important to bear in mind that flax fibers and the partially bio-based resin offer decreased footprint compared to conventional petroleum-derived matrices, *i.e.* epoxies, unsaturated polyesters, vinyl esters, phenol-formaldehyde resins, among other, and the typical reinforcing fibers in composites, *i.e.* carbon, aramid and glass fibers.

Acknowledgements.

This research was funded by the Ministerio de Economía, Industria y Competitividad (MICINN) project number MAT2017-84909-C2-2-R. D. Lascano wants to thank UPV for the grant received though the PAID-01-18 program. Microscopy services at UPV are acknowledged for their help in collecting and analyzing FESEM images.

Author Contributions.

Conceptualization, R.B and D.L.; methodology, D.G.-S.., T.B.; validation, A.A., D.L.; formal analysis, D.G.-S. and N.M.; investigation, D.L.; data curation, D.L, and A.A.; writing—original draft preparation, T.B. and R.B.; writing—review and editing, N.M.; supervision, R.B. and N.M.; project administration, R.B.

References.

[1] S. Yang, V. B. Chalivendra, and Y. K. Kim, *Composite Structures,* **168**, pp. 120-129, (2017).

[2] R. Rahman and S. Zhafer Firdaus Syed Putra, *Tensile properties of natural and synthetic fiber-reinforced polymer composites*: Elsevier Ltd, 2018.

[3] B. Song, T. Wang, L. Wang, H. Liu, X. Mai, X. Wang*, et al.*, *Composites, Part B,* **158**, pp. 259-268, (2019).

[4] C. Soutis, *Prog. Aeronaut. Sci.,* **41**, 2, pp. 143-151, (2005).

[5] R. A. Sullivan, *JOM,* **58**, 11, pp. 77-79, (2006).

[6] E. Monaldo, F. Nerilli, and G. Vairo, *Composite Structures,* (2019).

[7] Z. S. W. J. Yin, *Constr. Build. Mater.,* **17**, 6-7, pp. 463-470, (2003).

[8] D. Church, *Reinforced Plastics,* **62**, 1, pp. 35-37, (2018).

[9] S. E. Artemenko and Y. A. Kadykova, *Fibre Chem.,* **40**, 1, pp. 37-39, (2008).

[10] G. Marom, E. Drukker, A. Weinberg, and J. Banbaji, *Composites,* **17**, 2, pp. 150-153, (1986).

[11] A.-C. Corbin, D. Soulat, M. Ferreira, A.-R. Labanieh, X. Gabrion, P. Malécot*, et al.*, *Composites, Part B,* **181**, p. 107582, (2020).

[12] O. Faruk, A. K. Bledzki, H. P. Fink, and M. Sain, *Prog. Polym. Sci.,* **37**, 11, pp. 1552-1596, (2012).

[13] S. Shahinur and M. Hasan, *Natural Fiber and Synthetic Fiber Composites: Comparison of Properties, Performance, Cost and Environmental Benefits*: Elsevier Ltd., 2019.

[14] M. Ramesh, *Prog. Mater. Sci.,* **102**, pp. 109-166, (2019).

[15] Y. Zhang, Y. Li, H. Ma, and T. Yu, *Compos. Sci. Technol.,* **88**, pp. 172-177, (2013).

[16] S. S. Morye and R. P. Wool, *Polym. Compos.,* **26**, 4, pp. 407-416, (2005).

[17] M. Ramesh, C. Deepa, G. Arpitha, and V. Gopinath, *World J. Eng.,* (2019).

[18] P. K. Bajpai, K. Ram, L. K. Gahlot, and V. K. Jha, *Mater. Today: Proc.,* **5**, 2, pp. 8699-8706, (2018).

[19] K. Palanikumar, M. Ramesh, and K. Hemachandra Reddy, *J. Nat. Fibers,* **13**, 3, pp. 321-331, (2016).

[20] V. Fiore, T. Scalici, G. Di Bella, and A. Valenza, *Composites, Part B,* **74**, pp. 74-94, (2015).

[21] T. Czigány, J. Vad, and K. Pölöskei, *Period. Polytech., Mech. Eng.,* **49**, 1, pp. 3-14, (2005).

[22] T. Deák and T. Czigány, *Text. Res. J.,* **79**, 7, pp. 645-651, (2009).

[23] M. Birkner, S. Spange, and K. Koschek, *Polym. Compos.,* pp. 1-7, (2018).

[24] J. J. Lee, J. Song, and H. Kim, *Fibers Polym.,* **15**, 11, pp. 2329-2334, (2014).

[25] M. Tehrani Dehkordi, H. Nosraty, M. M. Shokrieh, G. Minak, and D. Ghelli, *Mater. Des.,* **43**, pp. 283-290, (2013).

[26] D. Matykiewicz, M. Barczewski, D. Knapski, and K. Skórczewska, *Composites, Part B,* **125**, pp. 157-164, (2017).

[27] D. Matykiewicz and M. Barczewski, *Composites Communications,* p. 100360, (2020).

[28] C. Sergi, J. Tirillò, M. C. Seghini, F. Sarasini, V. Fiore, and T. Scalici, *Polymers,* **11**, 4, p. 603, (2019).

[29] M. D. Samper, R. Petrucci, L. Sánchez-Nacher, R. Balart, and J. M. Kenny, *Polym. Compos.,* **36**, 7, pp. 1205-1212, (2015).

[30] B. V. Ramnath, C. Elanchezhian, P. V. Nirmal, G. P. Kumar, V. S. Kumar, S. Karthick*, et al.*, *Fibers Polym.,* **15**, 6, pp. 1251-1262, (2014).

[31] J. Yang, J. Xiao, J. Zeng, L. Bian, C. Peng, and F. Yang, *Fibers Polym.,* **14**, 5, pp. 759-766, (2013).

[32] Y. Xie, C. A. S. Hill, Z. Xiao, H. Militz, and C. Mai, *Composites, Part A,* **41**, 7, pp. 806-819, (2010).

[33] H. A. Al-Qureshi, *J. Mater. Process. Technol.,* **118**, 1-3, pp. 58-61, (2001).

[34] H. Kishi, A. Fujita, H. Miyazaki, S. Matsuda, and A. Murakami, *J. Appl. Polym. Sci.,* **102**, 3, pp. 2285-2292, (2006).
[35] W. Riemenschneider and H. M. Bolt, *Ullmann's Encycl. Ind. Chem.,* pp. 8676-8694, (2005).
[36] F. L. Jin, X. Li, and S. J. Park, *J. Ind. Eng. Chem.,* **29**, pp. 1-11, (2015).
[37] B. Ferrero, V. Fombuena, O. Fenollar, T. Boronat, and R. Balart, *Polym. Compos.,* **36**, 8, pp. 1378-1385, (2015).
[38] T. Boronat, V. Fombuena, D. Garcia-Sanoguera, L. Sanchez-Nacher, and R. Balart, *Mater. Des.,* **68**, pp. 177-185, (2015).
[39] A. Carbonell-Verdu, L. Bernardi, D. Garcia-Garcia, L. Sanchez-Nacher, and R. Balart, *Eur. Polym. J.,* **63**, pp. 1-10, (2015).
[40] S. Torres-Giner, N. Montanes, O. Fenollar, D. García-Sanoguera, and R. Balart, *Mater. Des.,* **108**, pp. 648-658, (2016).
[41] D. Lascano, J. Valcárcel, R. Balart, L. Quiles-Carrillo, and T. Boronat, *Ingenius,* 23, pp. 62-73, (2020).
[42] J. M. Park, W. G. Shin, and D. J. Yoon, *Compos. Sci. Technol.,* **59**, 3, pp. 355-370, (1999).
[43] J. Cruz and R. Fangueiro, *Procedia Eng.,* **155**, pp. 285-288, (2016).
[44] H. Luo, G. Xiong, C. Ma, P. Chang, F. Yao, Y. Zhu*, et al.*, *Polym. Test.,* **39**, pp. 45-52, (2014).
[45] M. Sood and G. Dwivedi, *Egypt. J. Pet.,* **27**, 4, pp. 775-783, (2018).
[46] M. D. Samper, R. Petrucci, L. Sánchez-Nacher, R. Balart, and J. M. Kenny, *Composites, Part B,* **71**, pp. 203-209, (2015).
[47] R. Petrucci, C. Santulli, D. Puglia, E. Nisini, F. Sarasini, J. Tirillò*, et al.*, *Composites, Part B,* **69**, pp. 507-515, (2015).
[48] R. Petrucci, C. Santulli, D. Puglia, F. Sarasini, L. Torre, and J. M. Kenny, *Mater. Des.,* **49**, pp. 728-735, (2013).
[49] R. Park and J. Jang, *Journal of Materials Science,* **34**, 12, pp. 2903-2910, (1999).
[50] L. V. J. Lassila, T. Nohrström, and P. K. Vallittu, *Biomaterials,* **23**, 10, pp. 2221-2229, (2002).
[51] F. Rezaei, R. Yunus, N. A. Ibrahim, and E. S. Mahdi, *Polym.-Plast. Technol. Eng.,* **47**, 4, pp. 351-357, (2008).
[52] D. Lascano, L. Quiles-Carrillo, R. Balart, T. Boronat, and N. Montanes, *Materials,* **12**, 4, pp. 622-622, (2019).
[53] D. Garcia-Garcia, J. M. Ferri, T. Boronat, J. Lopez-Martinez, and R. Balart, *Polym. Bull.,* **73**, 12, pp. 3333-3350, (2016).
[54] M. Evstatiev, S. Fakirov, B. Krasteva, K. Friedrich, J. A. Covas, and A. M. Cunha, *Polym. Eng. Sci.,* **42**, 4, pp. 826-835, (2002).
[55] I. D. G. Ary Subagia, Y. Kim, L. D. Tijing, C. S. Kim, and H. K. Shon, *Composites, Part B,* **58**, pp. 251-258, (2014).
[56] J. Zhang, K. Chaisombat, S. He, and C. H. Wang, *Mater. Des.,* **36**, pp. 75-80, (2012).
[57] J. M. España, M. D. Samper, E. Fages, L. Sánchez-Nácher, and R. Balart, *Polym. Compos.,* **34**, 3, pp. 376-381, (2013).
[58] D. Bertomeu, D. García-Sanoguera, O. Fenollar, T. Boronat, and R. Balart, *Polym. Compos.,* **33**, 5, pp. 683-692, (2012).
[59] J. Militký, V. Kovačič, and J. Rubnerová, *Eng. Fract. Mech.,* **69**, 9, pp. 1025-1033, (2002).
[60] P. Wambua, J. Ivens, and I. Verpoest, *Compos. Sci. Technol.,* **63**, 9, pp. 1259-1264, (2003).
[61] V. Fiore, G. Di Bella, and A. Valenza, *Mater. Des.,* **32**, 4, pp. 2091-2099, (2011).
[62] G. Romhány, J. Karger-Kocsis, and T. Czigány, *J. Appl. Polym. Sci.,* **90**, 13, pp. 3638-3645, (2003).
[63] M. S. M. Jusoh, C. Santulli, M. Y. M. Yahya, N. Hussein, and H. A. I. Ahmad, *Mater. Sci. Eng. Adv. Res,* **1**, 4, pp. 19-25, (2016).

[64] B. H. Jones, D. R. Wheeler, H. T. Black, M. E. Stavig, P. S. Sawyer, N. H. Giron*, et al.*, *Macromolecules,***50**, 13, pp. 5014-5024, (2017).
[65] R. A. Pethrick, E. A. Hollins, I. McEwan, E. A. Pollock, D. Hayward, and P. Johncock, *Polymer International,***39**, 4, pp. 275-288, (1996).
[66] V. B. Gupta, J. Rich, L. T. Drazal, and C. Y. C. Lee, **25**, 13, (1985).
[67] P. Czub, *Macromol. Symp.,***242**, pp. 60-64, (2006).
[68] R. J. Varley, W. Tian, K. H. Leong, A. Y. Leong, F. Fredo, and M. Quaresimin, *Polym. Compos.,***34**, 3, pp. 320-329, (2013).
[69] V. B. Gupta and C. Brahatheeswaran, *Polymer,***32**, 10, pp. 1875-1884, (1991).

Table captions

Table 1. Physical properties of flax and basalt fibers and their corresponding fabrics used for composite manufacturing.

Table 2. Composition and stacking sequence of hybrid composite laminates with different basalt/flax plies.

Table 3. Mechanical properties of basalt/flax hybrid composite laminates with different stacking sequences obtained from flexural and Charpy tests.

Table 4. Mechanical properties of basalt/flax hybrid composite laminates with different stacking sequences obtained tensile tests on notched samples (U type).

Table 5. Thermomechanical properties basalt/flax hybrid laminate composites obtained by dynamic mechanical thermal analysis (DMTA) and thermomechanical analysis (TMA).

Table 1. Physical properties of flax and basalt fibers, and their corresponding fabrics used for composite manufacturing.

Properties	**Basalt fibers**	**Flax fiber**
Density od unsized filament (kg dm^{-3})	2.67	1.5
Moisture content (%)	0.1	-
Melting point (ºC)	1350	-
Weave type	Twill 2/2	Twill 2/2
Fiber diameter (µm)	17	20
Young Modulus (GPa)	85	50
Yarn density: warp (ends cm^{-1})	3.8	7
Yarn density: weft (ends cm^{-1})	3.8	7
Ply thickness (mm)	0.53	0.6-0.8

Table 2. Composition and stacking sequence of hybrid composite laminates with different basalt/flax plies.

Code	**Ply number ratio (basalt/flax)**	**Stacking Sequence**	**Image view of the cross section**
B8F0	8/0		
B6F2	6/2		
B4F4	4/4		
B2F6	2/6		
B4F4alt	4/4		
B0F8	0/8		

Basalt fabric ply Flax fabric ply

Table 3. Mechanical properties of basalt/flax hybrid composite laminates with different stacking sequences obtained from flexural and Charpy tests.

Code	**Flexural properties**		**Impact strength (kJ m^{-2})**
	σ_f (MPa)	**E_f (GPa)**	
B8F0	467.9±83.3[a]	14.7±1.0[a]	116.9±2.1[a]
B6F2	307.7±53.9[a]	12.2±0.7[b,a]	88.0±5.7[b]
B4F4	241.9±39.6[b]	9.5±0.4[c]	64.0±4.8[d,e]
B2F6	129.7±24.7[c,d]	6.4±0.4[d]	58.1±1.2[e,d]
B4F4alt	156.5±28.6[d,c]	4.0±0.2[e]	77.8±5.0[c]
B0F8	51.5±10.2[e]	2.2±0.1[f]	9.0±0.8[f]

[a-f] different letters in the same column indicate a significant difference among the samples $p<0.05$

Table 4. Mechanical properties of basalt/flax hybrid composite laminates with different stacking sequences obtained tensile tests on notched samples (U type).

Code	**σ_t (MPa)**	**ε_b (%)**	**Area (MN m m^{-3})**
B8F0	211.9±13.8[a]	23.0±0.8[a]	25.06±2.03[a]
B6F2	146.8±18.1[b]	21.1±2.8[a,c]	15.41±1.24[b]
B4F4	104.8±12.9[c]	19.7±0.5[b,c,a]	9.69±1.02[c]
B2F6	54.9±12.8[e]	11.4±3.0[d]	3.39±0.31[d]
B4F4alt	85.9±5.4[d]	18.3±1.0 [c,b,a]	5.65±0.49[e]
B0F8	21.7±6.8[f]	16.2±3.5[c,b,a]	1.77±0.15[f]

[a-f] different letters in the same column indicate a significant difference among the samples $p<0.05$

Table 5. Thermomechanical properties basalt/flax hybrid laminate composites obtained by dynamic mechanical thermal analysis (DMTA) and thermomechanical analysis (TMA).

Code	**DMTA results**			**CLTE (μm m^{-1} K^{-1}) by TMA**	
	T_g (°C)	***G′* at 60 °C (GPa)**	***G′* at 125 °C (MPa)**	**Below T_g**	**Above T_g**
B8F0	90.1±1.8^{a}	1.78±0.04^{a}	98.4±2.0^{a}	260.9±17.2^{a,b}	296.0±17.0^{a,b}
B6F2	91.1±2.0^{a}	1.47±0.03^{b}	69.3±1.7^{b}	256.1±21.0^{a,b}	323.6±18.8^{a}
B4F4	91.8±2.1^{a}	1.07±0.03^{d}	64.9±1.1^{c}	245.7±19.2^{b,a}	367.8±19.2^{c}
B2F6	90.4±2.3^{a}	1.37±0.05^{c}	91.3±2.2^{a}	254.2±21.8^{a,b}	320.6±17.1^{a}
B4F4alt	90.4±1.3^{a}	1.35±0.04^{c}	62.3±1.6^{c}	260.3±22.8^{a,b}	376.9±22.1^{c}
B0F8	90.9±1.5^{a}	0.57±0.01^{e}	26.6±0.5^{d}	250.9±20.3^{a,b}	273.2±20.7^{b,a}

$^{a-e}$ different letters in the same column indicate a significant difference among the samples $p<0.05$

Figure captions

Figure 1. Detail of "U" type notched samples for Charpy test to evaluate the impact strength of hybrid composite laminates with different basalt/flax plies with a partially bio-based epoxy resin.

Figure 2. Field emission scanning electron microscopy (FESEM) images at different magnifications (x200 left column, x1000 right column) corresponding to surface morphology of (a)-(b) As-received basalt fibers, (c)-(d) Untreated flax fibers, (e)-(f) Basalt fibers subjected to cleaning + heat treatment, (g)-(h) Silanized basalt fibers and (i)-(j) silanized flax fibers.

Figure 3. Stress-strain curve plots of notched samples (U type) of basalt/flax hybrid composite laminates with different stacking sequences obtained from tensile tests.

Figure 4. Field emission scanning electron microscopy (FESEM) images at different magnifications (200x left column, 500x right column) corresponding to fractured surfaces from impact tests of composites with different fibers embedded into an epoxy resin matrix, (a)-(b) all-basalt B8F0 composite plate, (c)-(d) all-flax B0F8 composite plate.

Figure 5. Stereomicroscopy images at different magnifications (X16, left and central column; X40 right column) corresponding to the cross section and the fracture surfaces from impact tests of (a)-(b) -(c) B8F0, (d)-(e) -(f) B6F2, (g)-(h) -(i) B4F4, (j)-(k) -(l) B2F6, (m)-(n) -(o) B4F4alt, (p)-(q) -(r) B0F8.

Figure 6. Dynamic mechanical thermal analysis (DMTA) behaviour of hybrid basalt/flax composite laminates with different stacking sequences, (a) storage modulus – *G′* and (b) dynamic damping factor, *tan* (δ).

Figure 1. Detail of “U” type notched samples for Charpy test to evaluate the impact strength of hybrid composite laminates with different basalt/flax plies with a partially bio-based epoxy resin.

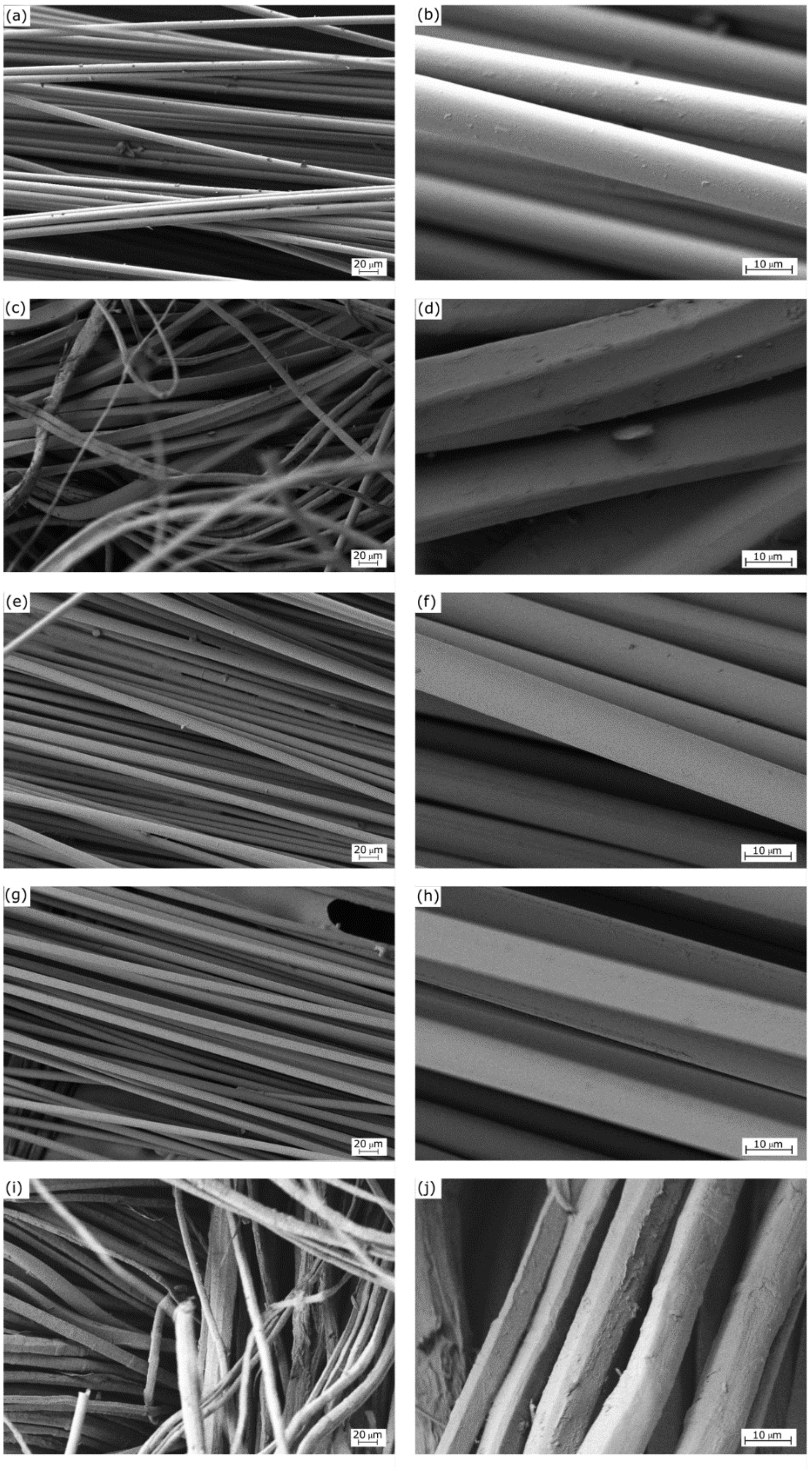

Figure 2. Field emission scanning electron microscopy (FESEM) images at different magnifications (x200 left column, x1000 right column) corresponding to surface morphology of (a)-(b) As-received basalt fibers, (c)-(d) Untreated flax fibers, (e)-(f) Basalt fibers subjected to cleaning + heat treatment, (g)-(h) Silanized basalt fibers and (i)-(j) silanized flax fibers.

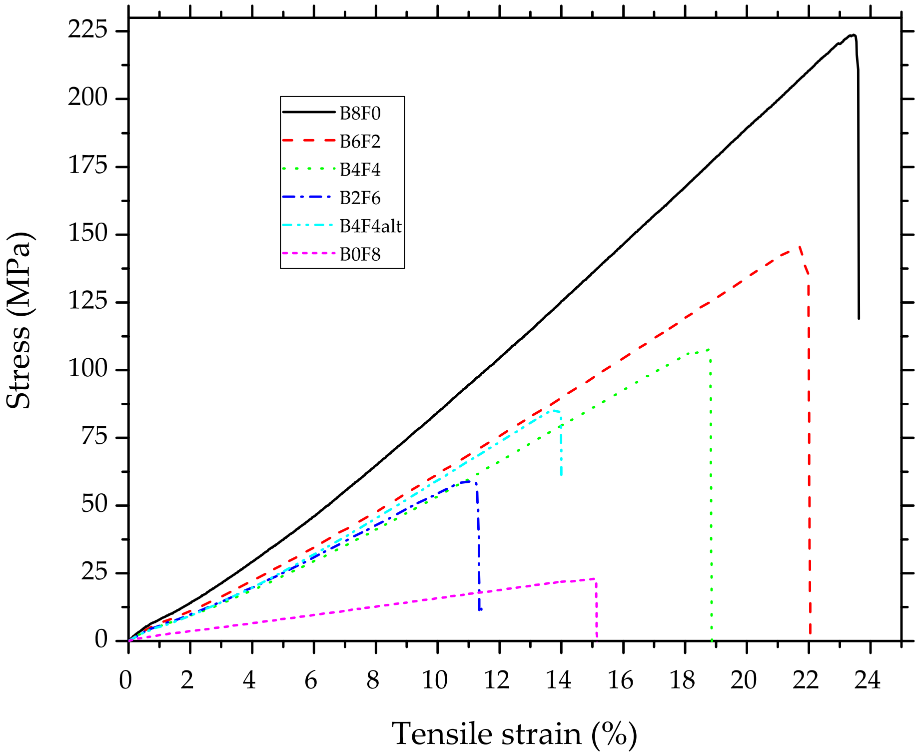

Figure 3. Stress-strain curve plots of notched samples (U type) of basalt/flax hybrid composite laminates with different stacking sequences obtained from tensile tests.

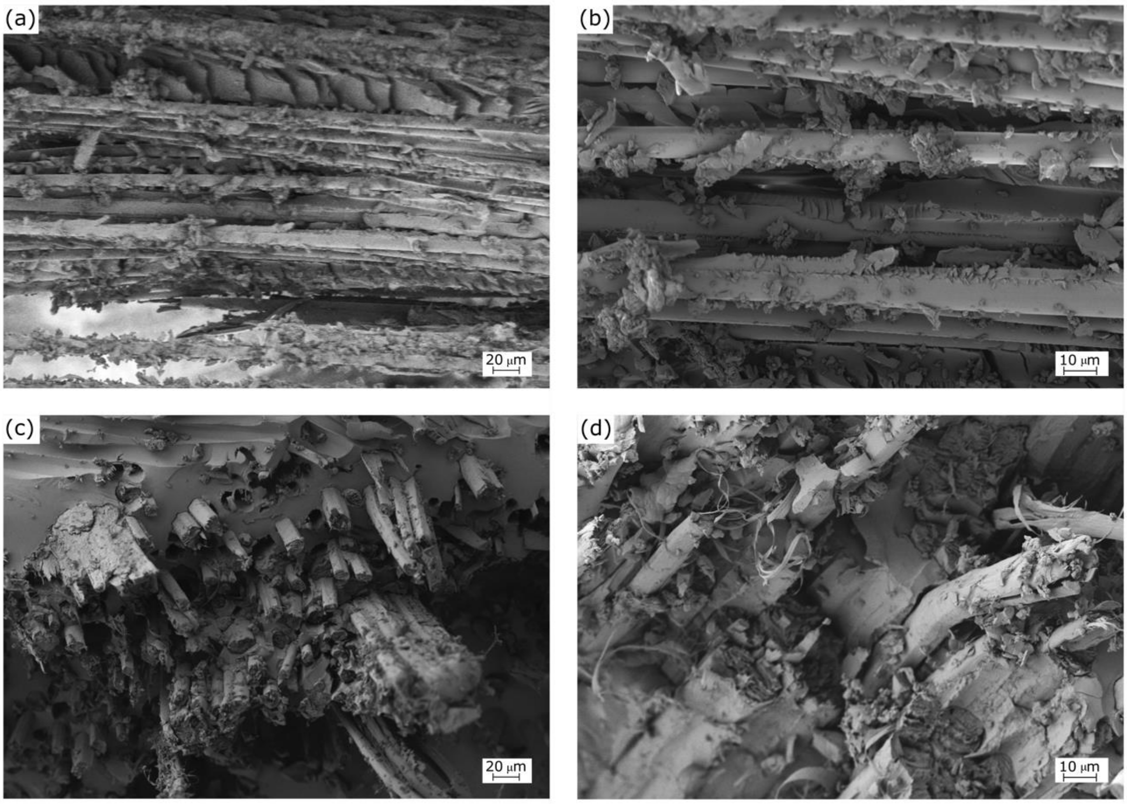

Figure 4. Field emission scanning electron microscopy (FESEM) images at different magnifications (200x left column, 500x right column) corresponding to fractured surfaces from impact tests of composites with different fibers embedded into an epoxy resin matrix, (a)-(b) all-basalt B8F0 composite plate, (c)-(d) all-flax B0F8 composite plate.

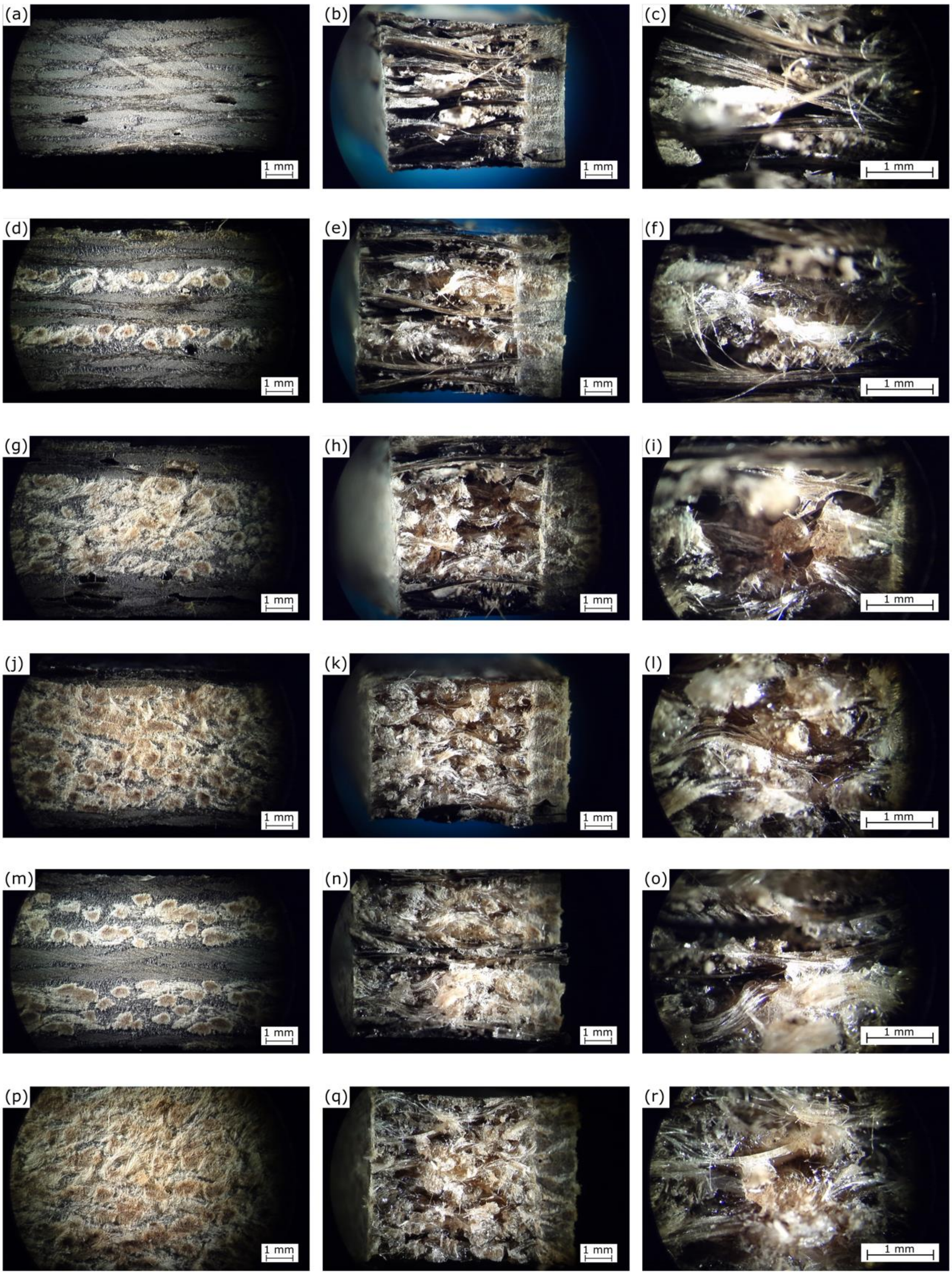

Figure 5. Stereomicroscopy images at different magnifications (X16, left and central column; X40 right column) corresponding to the cross section and the fracture surfaces from impact tests of (a)-(b) -(c) B8F0, (d)-(e) -(f) B6F2, (g)-(h) -(i) B4F4, (j)-(k) -(l) B2F6, (m)-(n) -(o) B4F4alt, (p)-(q) -(r) B0F8.

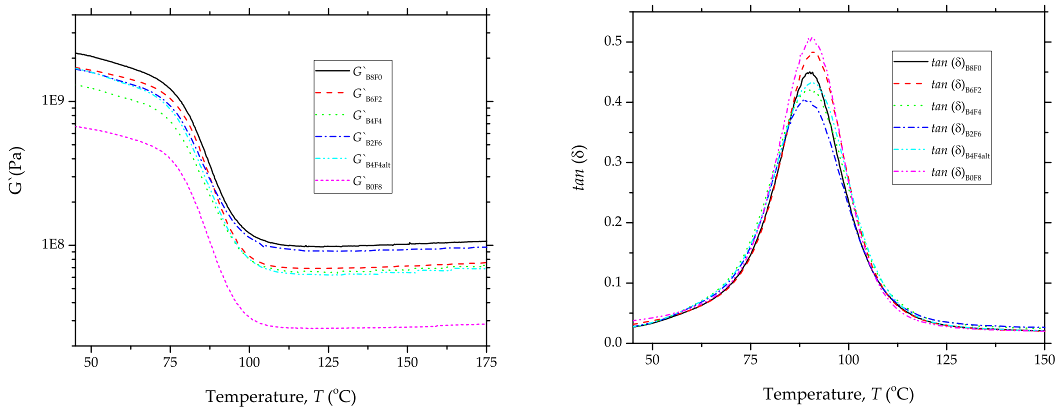

(a) (b)

Figure 6. Dynamic mechanical thermal analysis (DMTA) behaviour of hybrid basalt/flax composite laminates with different stacking sequences, (a) storage modulus – *G′* and (b) dynamic damping factor, *tan* (δ).

Scheme captions

Scheme 1. Stages of the vacuum assisted resin infusion molding (VARIM) of hybrid composite laminates with different basalt/flax plies with a partially bio-based epoxy resin. a) Defining the stacking sequence, b) Adding the peel-ply and bleeding fabric, c) Testing the vacuum level to check no leakage and d) Resin infusion assisted by vacuum.

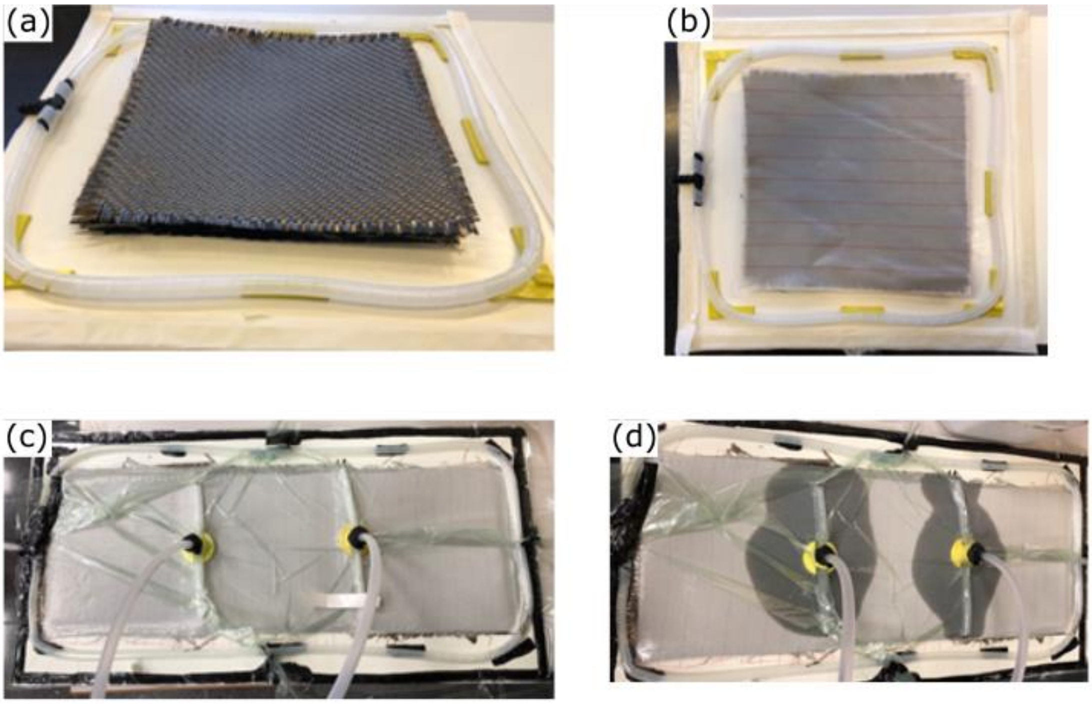

Scheme 1. Stages of the vacuum assisted resin infusion molding (VARIM) of hybrid composite laminates with different basalt/flax plies with a partially bio-based epoxy resin. a) Defining the stacking sequence, b) Adding the peel-ply and bleeding fabric, c) Testing the vacuum level to check no leakage and d) Resin infusion assisted by vacuum.